Available online at www.sciencedirect.com
ScienceDirect
Cement and Concrete Research 37 (2007) 844–855
Cement and Concrete Research

Chemical interactions between siliceous aggregates and low-Ca alkali-activated cements

W.K.W. Lee, J.S.J. van Deventer *

Department of Chemical and Biomolecular Engineering, The University of Melbourne, Victoria 3010, Australia

Received 17 March 2007; accepted 26 March 2007

Abstract

The chemical interactions between natural siliceous aggregates and a low-Ca alkali-activated cement (geopolymer) were studied. By leaching ideal aluminosilicate minerals such as kaolinite and albite in various alkaline solutions with or without soluble silicates, it was found that addition of 0.5 M SiO_2 to a highly alkaline activating solution ($[OH^-]_0$=5 to 10 M) was responsible for the formation of an Al-enriched aluminosilicate surface through the initial non-stoichiometric and Si preferential dissolution of the parent aluminosilicates. This then facilitated soluble silicate deposition from the activating solutions onto the Al-rich surfaces, which resulted in the formation of a dense deposited aluminosilicate gel interfacial layer. This aluminosilicate interface formed during albite leaching ($[OH^-]_0$=5 to 10 M and $[SiO_2]_0$=0.5 M) was found to possess a similar Si/Al ratio to the real interface between a siliceous aggregate slice (basalt or siltstone) and a low-Ca fly ash/kaolinite geopolymer, activated with an activating solution of $[OH^-]_0$=10 M and $[SiO_2]_0$=2.5 M. Due to the similarities between the activating solutions used and the interfaces formed, it is postulated that a similar formation mechanism is shared between the deposited aluminosilicate interface formed from leaching and a 'real' geopolymer concrete synthesis. Without soluble silicate addition, or if a solution of low alkalinity ($[OH^-]_0$=0.6 M and $[SiO_2]_0$=0 and 0.5 M) was used, the Al-enriched reacting surface was not formed, and no deposited aluminosilicate interface was observed in these systems.

Keywords: Aggregate; Alkali activated cement; Interfacial transition zone; Microstructure

1. Introduction

Alkali-activation of aluminosilicate solids using alkaline hydroxide and/or silicate solutions can be used to synthesise inorganic geopolymeric binders, or alkali-activated cements, displaying excellent physical and chemical properties [1–4]. Experimental evidence suggests that the principal binding phase within geopolymers, where low-Ca source materials are used, is an X-ray amorphous aluminosilicate gel consisting of a three-dimensional framework of SiO_4 and AlO_4 tetrahedra linked by corner-shared O atoms [1,3]. The negatively-charged tetrahedral Al sites in the network are charge-balanced by alkali metal cations such as Na^+ and/or K^+. This aluminosilicate gel can be used to bind various mineral aggregates, such as sand, natural rock and/or other mineral fragments to produce mortars and concretes. On the other hand, if the raw material used is rich in Ca, such as a blast furnace slag, there is growing evidence to suggest that the binding phase formed is a mixture of calcium silicate hydrate (CSH) and aluminosilicate gels, whose relative proportions can be determined to a certain extent by the abundance of Ca from the source materials and the stoichiometry of the reaction(s) [5–7].

It is well known that in early ordinary Portland cement (OPC) concrete, before setting, the region close to the aggregate surface has on average less cement grains and is instead filled to a significant extent with water. This water-rich region is approximately 50 μm thick [8], similar to the thickness of the interfacial transition zone (ITZ) in mature OPC mortars and concretes [9]. Dissolved ions therefore must diffuse from the nearby cement particles to this region if the aggregate is chemically inert. According to some investigators, the differential diffusion of Ca^{2+} relative to Si^{4+} in a hydrating Portland cement system is responsible for the higher calcium hydroxide concentration observed in the ITZ than in the bulk cement gel [10,11].

There is, however, increasing evidence suggesting that mineral aggregates do chemically interact with the cement pore solution. Tasong *et al.* [12] reported that siliceous rocks

* Corresponding author. Tel.: +61 3 83446619; fax: +61 3 83447707.
E-mail address: jannie@unimelb.edu.au (J.S.J. van Deventer).

0008-8846/$ - see front matter © 2007 Elsevier Ltd. All rights reserved.
doi:10.1016/j.cemconres.2007.03.012

such as basalt and quartzite, and silica sand, could absorb 'significant' amounts of OH^- and Ca^{2+} from an artificial cement solution (~70 mM of OH^-, ~6 mM of Na^+, ~36 mM of K^+, and ~4 mM of Ca^{2+}). Si^{4+} was found to dissolve from the aggregates initially and then start to precipitate after a period of time. These results suggest that heterogeneous nucleation of calcium hydroxide could originate at the aggregate surface, as has also been reported by other investigators [10,13]. Calcium silicate hydrates (C–S–H) could then form at or near this calcium hydroxide layer at the aggregate surface after the solubility limit with respect to C–S–H is reached. This implies that the C–S–H within the ITZ, and to some degree in the bulk cement paste as well, could be comprised in part of the Si^{4+} dissolved from both the cement and the siliceous aggregates.

In alkali-activated cement systems, it is often speculated that the extent of chemical interactions between siliceous aggregates and the highly alkaline 'activating' solutions can be significant. As soluble silicates are often used to improve the physical and chemical performances of alkali-activated cements [1–3], the reactions that take place between siliceous minerals and the alkaline silicate solutions can be very different from those using alkaline solutions without additional soluble silicates. Although some work has been conducted to examine Ca-rich geopolymer systems using slag as the solid raw material or blended with OPC [5–7], relatively little attention that has been paid to understanding the chemical reactions at the interface with a siliceous aggregate. This paper therefore aims to examine the chemical interactions of rock-forming crystalline aluminosilicate minerals and natural siliceous rocks with alkaline solutions, with and without additional soluble silicates. The bonding mechanisms between rock aggregates and low-Ca alkali activated cements will also be discussed.

2. Experimental methods

2.1. Materials

Gladstone fly ash (Class F according to ASTM C618, d_{50}=14.1 μm) was obtained from Queensland Cement Limited, Australia. Kaolinite (HR1 grade, d_{50}=0.47 μm) was obtained from Commercial Minerals, Sydney, Australia. The compositions as determined by fusion analysis using a Siemens SRS3000 sequential X-ray fluorescence (XRF) spectrometer are listed in Table 1. The major crystalline components of the fly ash observed in X-ray diffraction (XRD) analysis (Phillips PW 1800, CuK_α radiation) are α-quartz, mullite, hematite and magnetite. The major crystalline components of the HR1 grade kaolinite as supplied are kaolinite and α-quartz. From the compositions presented in Table 1 and by taking account of the ideal chemical formula of kaolinite ($Al_2Si_2O_5(OH)_4$), the kaolinite sample used in this investigation is estimated to contain ~88 wt% of pure kaolinite and ~12 wt% of quartz, assuming all the excess SiO_2 is crystalline. Similarly, the albite used ($NaAlSi_3O_8$, d_{50}=4.5 μm, Minerals Corporation Limited, Broken Hill, Australia) is estimated to contain ~97 wt% pure albite with ~3 wt% of a quartz impurity. The Brunauer–Emmett–Teller (BET) surface area, calculated using a six-point nitrogen adsorption method (Micromeritics ASAP 2000), is 15.7 $m^2\ g^{-1}$ for the kaolinite and 0.24 $m^2\ g^{-1}$ for the albite. Sodium silicate solution (Vitrosol N(N40), molar ratio SiO_2/Na_2O=3.32, [SiO_2]=6.63M) was supplied by PQ Australia. Laboratory-grade NaOH and KOH reagents were obtained from Ajax Chemicals Australia. Distilled/deionised water was used throughout the research.

Table 1
The mass compositions of the raw materials

Oxide	Fly ash (wt %)	Kaolinite (wt %)	Albite (wt %)	Basalt (wt %)	Siltstone (wt %)
SiO_2	50.0	54.5	70.9	48.4	81.3
Al_2O_3	28.0	29.4	17.5	13.8	7.2
Fe_2O_3	12.0	1.4	0.07	11.7	4.0
CaO	3.5	0.2	0.31	9.0	0.9
MgO	1.3	0.2	0.04	10.3	1.8
Na_2O	0.2	0.1	9.75	3.6	0.9
K_2O	0.7	0.2	0.43	1.0	1.4
TiO_2	1.7	2.8	0.05	1.9	0.7
Other minor oxides	0.6	0.2	0.2	0.3	0.2
Combustibles	2.0	11.0	0.75	0.0	1.6
Total	100.0	100.0	100.0	100.0	100.0

Basalt rocks with a pale grey appearance were obtained from Australian Slate Co., Melbourne, Australia. According to XRD and optical microscopy, the basalt rock comprised predominantly plagioclase feldspar (albite, disordered anorthite), potash feldspar (disordered sanidine), pyroxene (augite) and quartz, with a minor quantity of clay (kaolinite) filling the vesicles. The siltstone rock (Doncaster Quarry, Melbourne, Australia) was grey in appearance and comprised predominantly quartz and chlorite (clinochlore), with minor quantities of mica (muscovite and illite), clay (kaolinite) and plagioclase feldspar (disordered albite). The elemental compositions of the rocks used are listed in Table 1. The rocks were pulverised (basalt, d_{50}=4.7 μm; siltstone, d_{50}=5.1 μm) before leaching to increase the surface area per mass.

2.2. Synthesis of the low-Ca alkali-activated cement

A single geopolymer binder composition was used throughout the investigation, to enable observation of binding to the natural siliceous rocks without complications due to different gel chemistries. An alkaline activating solution with 10 M MOH (M=Na and K, Na:K=0.2:1) and 2.5 M soluble silicates ([SiO_2]=2.5 M) was prepared and allowed to cool to room temperature with stirring before binder synthesis. Fly ash and kaolin were mixed at a 9:1 mass ratio in a rotary mixer overnight. Then activating solution was added to the solid mixture at a liquid/solid mass ratio of 0.5, and mixed for 5 min with a mechanical mixer. The specimens used for the examination of the interface between the rocks and the alkali-activated cement were prepared by firstly cutting the rocks into slices as shown in Fig. 1. The rock surfaces were then lightly polished to minimise variations in surface roughness. The binder was then poured and compacted between two rock slices as in Fig. 1. The sandwich products were cured at 40±3 °C for

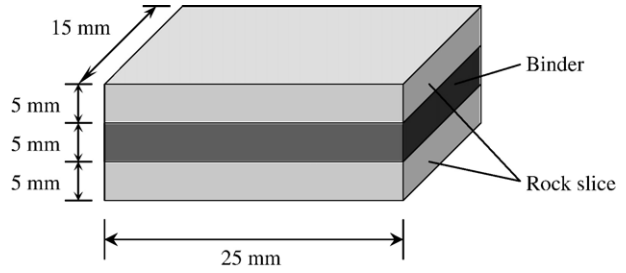

Fig. 1. Sandwich specimen geometry used for examining the interface between rock slices and a low Ca alkali-activated cement binder.

24 h and then demoulded. The samples were then cured at 25±3 °C and a relative humidity of 50±5% at atmospheric pressure until testing.

2.3. Leaching experiments

Mineral dissolution and precipitation reactions were studied by following the evolution of the dissolved Si and Al concentrations in batch reactors. Leaching solutions of various compositions were prepared according to Table 2, using Vitrosol N(N40) sodium silicate solution, NaOH and/or KOH and distilled/deionised water in the appropriate proportions. No additional buffering was used as the pH of all experiments was found to stay within±1 pH unit. These solutions were equilibrated to 25±0.5 °C with stirring before leaching was commenced. For each leaching experiment, 100 g of the minerals or the pulverized rocks was added to 1000 mL of the activating solution. The slurries were stirred at 25±0.5 °C with minimum agitation (150 rpm) to prevent sedimentation. At designated time intervals, 10 mL of the suspension was collected, diluted and separated using the procedure described previously [14]. The separated reacted solids were subsequently washed with ten increments of 20 mL distilled/deionised water and then once with 5 mL of ethanol, to remove the physically adsorbed species such as alkali cations and/or soluble silicates.

Table 2
The calculated molar compositions of the activating solutions for leaching

System	Activating solution		Solid
	$[OH^-]_0$ (M)	$[SiO_2]_0$ (M)	
Kao 1	0.6	0	Kaolinite
Kao 2	0.6	0.5	Kaolinite
Kao 3	5	0	Kaolinite
Kao 4	5	0.5	Kaolinite
Kao 5	10	0	Kaolinite
Kao 6	10	0.5	Kaolinite
Alb 1	0.6	0	Albite
Alb 2	0.6	0.5	Albite
Alb 3	5	0	Albite
Alb 4	5	0.5	Albite
Alb 5	10	0	Albite
Alb 6	10	0.5	Albite
B 1	0.6	0	Basalt
B 2	0.6	0.5	Basalt
B 3	5	0	Basalt
B 4	5	0.5	Basalt
B 5	10	0	Basalt
B 6	10	0.5	Basalt

2.4. Analysis

Inductively coupled plasma-optical emission spectroscopy (ICP-OES, Perkin-Elmer 3000) was used to determine Si, Al, Ca and Mg levels in the leach solution. The leached solids were also analysed by XRD. Fourier transform infrared (FTIR) spectra were acquired using a Bio-Rad FTS 165 FTIR spectrometer in absorbance mode using the KBr pellet technique (0.5 mg sample with 250 mg KBr). Pellets of samples were prepared using the normal procedure, dried in an oven at 60 °C overnight and pressed again before spectra were taken. All spectra were obtained with a sensitivity of 8 cm^{-1} and 64 scans per spectrum taken. The baseline of each spectrum was corrected for easier peak interpretation. Scanning electron microscopy (SEM) was conducted using a Phillips XL30 SEM microscope coupled with an Oxford Instruments energy dispersive spectrometer (EDS) with backscattered electron (BSE) and secondary electron (SE) detections. SEM-EDS line scan was used to measure the elemental concentration gradients across the interface between natural siliceous rocks and the AAC. This enabled estimation of the thickness of the interface, as will be discussed in the next section. The intervals were chosen so that at least 10 individual spot analyses were taken within a 5 μm distance each. The results of the SEM-EDS line scans presented in this work are all averages of 5 separate analyses at different locations. The locations of these line scans were carefully selected so as to avoid visible fly ash particles and other mineral fragments within the aluminosilicate gel as demonstrated in Fig. 2.

3. Results and discussion

3.1. The interface between siliceous rocks and low-Ca alkali activated cements

Typical morphological features of the interface between the natural siliceous rocks (basalt and siltstone) and the low Ca

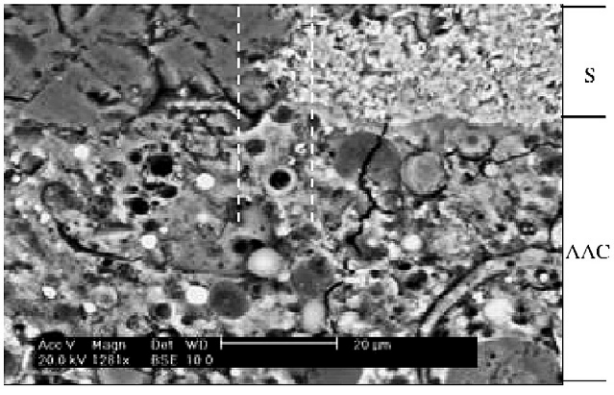

Fig. 2. BSE-SEM image of the siltstone sandwich specimen. S=siltstone slice, AAC=low-Ca alkali-activated cement. The locations where the SEM-EDS analyses were taken are marked as white dotted lines.

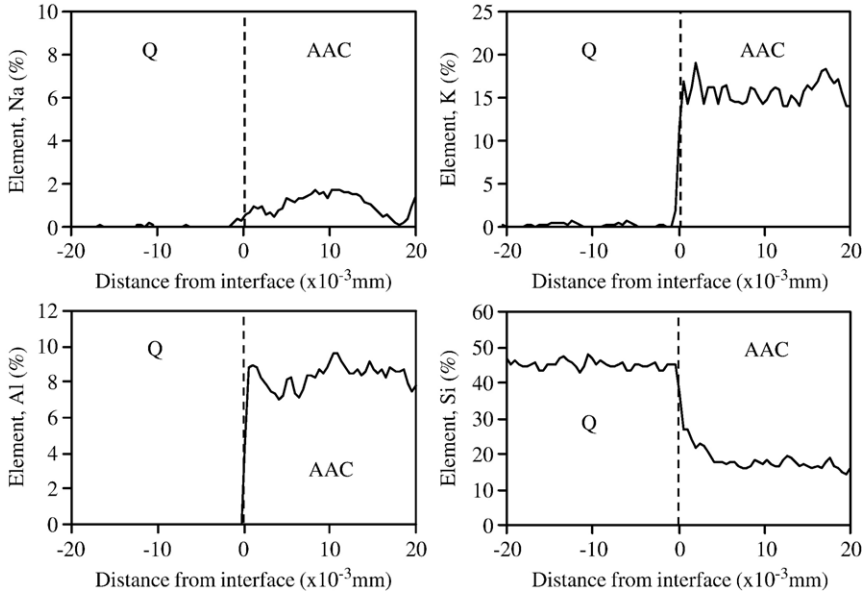

Fig. 3. SEM-EDS line scan results across the interface of quartz (Q) and alkali-activated cement (AAC) from the siltstone sandwich specimen.

geopolymer are presented in Fig. 2. The aluminosilicate geopolymeric gel in proximity to the rock surfaces morphologically resembles the bulk gel. No apparent crystalline interfacial products could be identified and it appears that good cohesion and bonding did exist between the rocks and the low-Ca alkali-activated cement. This is very different from OPC systems, where the interface (ITZ) is characterised by a higher concentration of $Ca(OH)_2$ and ettringite crystals [8–10]. More information about the mineral-binder interface can be gained from the SEM-EDS line scans in Figs. 3–6.

From Fig. 3, the concentration of Si was constant throughout the entire quartz structure whereas there was an abrupt decrease in Si concentration at the interface (the interface was identified by matching the morphological features of the SEM micrographs with the results of the SEM-EDS line scan). This indicates that very limited Si dissolution was present, possibly because penetration of alkali (Na^+ and K^+, accompanied by OH^-) into the quartz mineral was not extensive (Fig. 3). At the binder side of the interface, on the other hand, there was a Si concentration gradient from a maximum of ~28% at the quartz surface to a minimum of ~18% in the bulk gel, which occurred within a distance of ~5 μm. It must be noted that sufficient points were taken during each line scan (at least 10 individual spot analyses were taken within a 5 μm distance, see Section 2.4) to ensure that the concentration gradient detected was genuine. Similar Si concentration gradients, all within 5 μm or

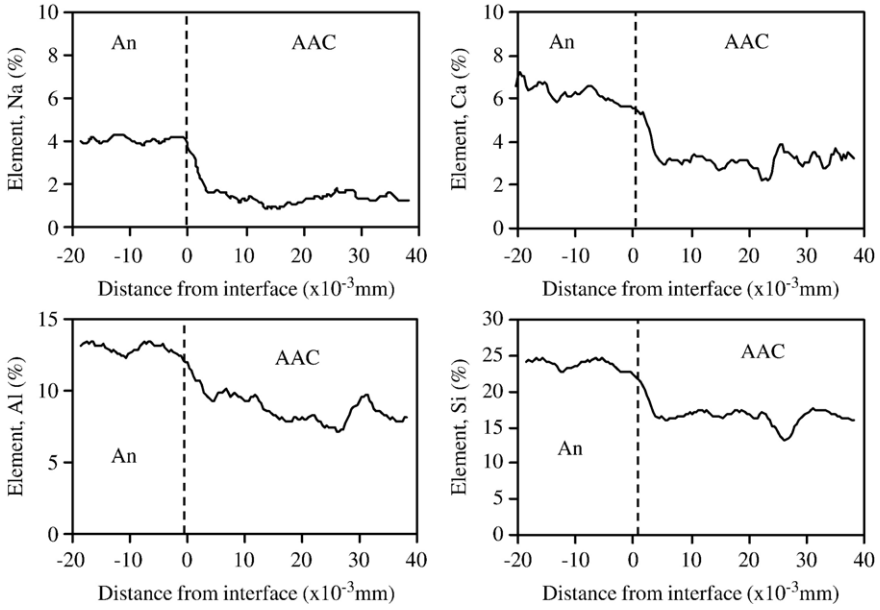

Fig. 4. SEM-EDS line scan results across the interface of anorthite (An) and alkali-activated cement (AAC) from the basalt sandwich specimen.

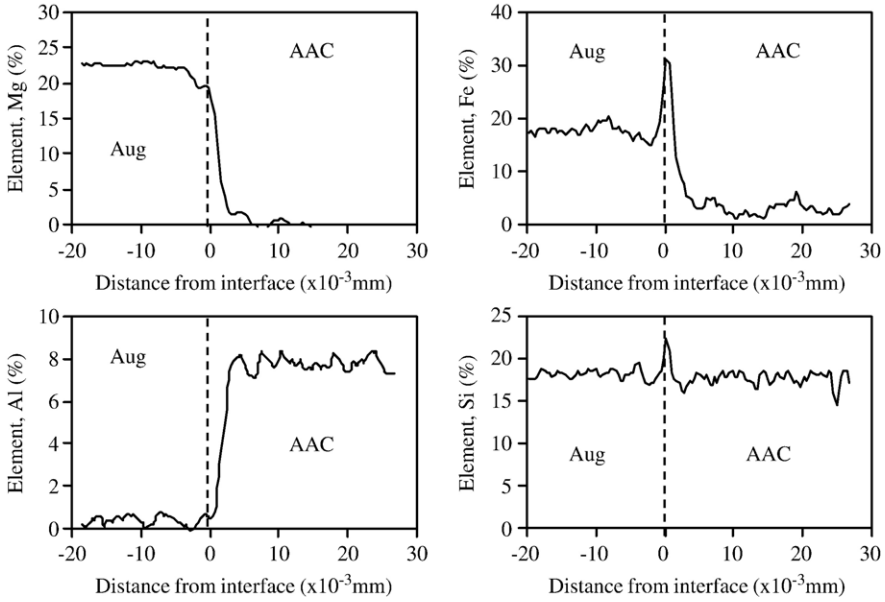

Fig. 5. SEM-EDS line scan results across the interface of augite (Aug) and alkali-activated cement (AAC) from the basalt sandwich specimen.

less, were also observed at other parts of the rock surfaces, where the Si concentration was always higher at the mineral surfaces such as albite (~21%, not shown), anorthite (~24%, Fig. 4), sanidine (~27%, not shown), augite (~23%, Fig. 5) and clinochlore (~23%, Fig. 6) than in the bulk gel (~18%). As the Si concentration is increasing continuously from the bulk gel to the rock surfaces, it is likely that Si is either dissolved away from the siliceous minerals or preferentially adsorbed onto the mineral surfaces from the activating solution containing soluble silicates, or both. This will be further examined in the next section, using leaching at increased liquid/solid ratios as a model for alkali activation of aluminosilicates.

Figs. 3–6 also appear to show that the aluminosilicate minerals network-modified by non-Group I cations such as Mg, Ca and Fe (anorthite, augite and clinochlore) are prone to alkali corrosion. Concentration gradients of the network modifiers (Mg, Ca and Fe) were found within the rock-forming minerals near the interfacial layer described above, which describes the region of Si concentration gradient near the surfaces of the siliceous minerals. These network modifier concentration gradients indicated that the network modifiers were leached out from the silicate structure during alkali activation. Hence, siliceous rocks are not chemically inert in low-Ca geopolymer systems, as is also the case in OPC systems [12]. The SEM-EDS study shown in Figs. 3–6 also

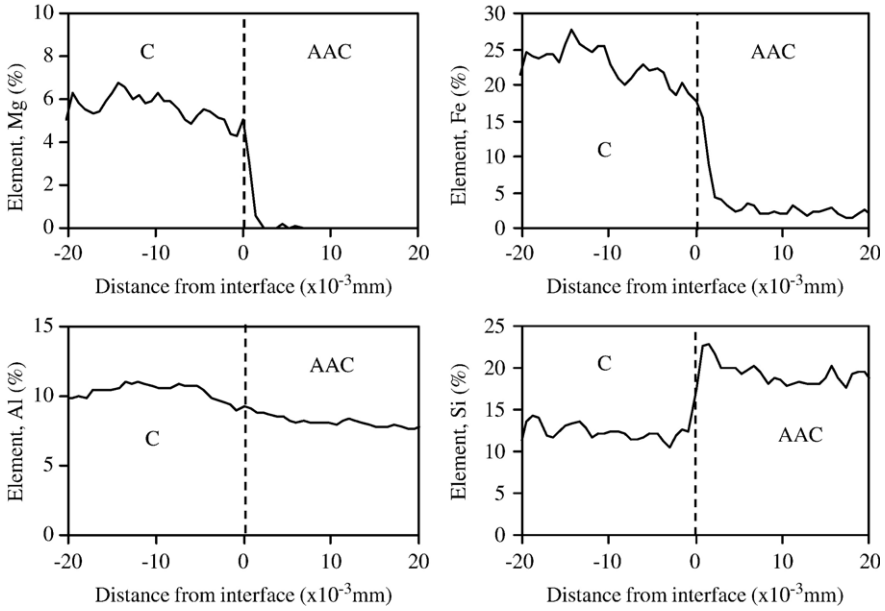

Fig. 6. SEM-EDS line scan results across the interface of clinochlore (C) and alkali-activated cement (AAC) from the siltstone sandwich specimen.

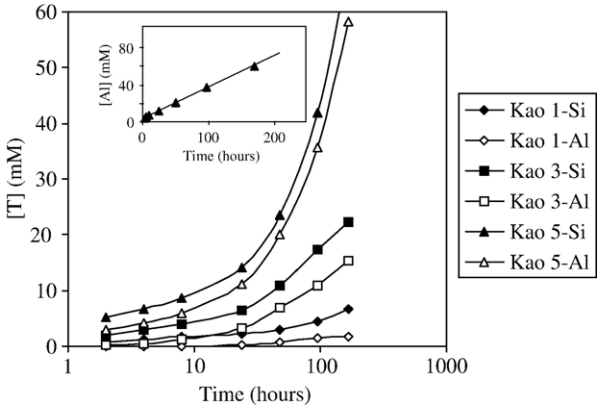

Fig. 7. Leaching behaviour of kaolinite in alkaline hydroxide solutions with $[OH^-]$=0.6 M (*Kao 1*), 5 M (*Kao 3*) and 10 M (*Kao 5*). [*T*]=concentration of Si or Al in the solution. Inset shows the linear leaching.

suggests that the chemical distinction denoting the interfacial layer between a siliceous rock and the gel binder is highly localised. For example, the interfacial layer of the siltstone sandwich sample, shown in Fig. 2, had an average molar composition of approximately $1.5Na_2O{\cdot}1.6MgO{\cdot}CaO{\cdot}[KAlO_2{\cdot}(SiO_2)_{2.6}]_{10}{\cdot}4.4Fe_2O_3{\cdot}xH_2O$ at the clinochlore surface (assuming all the Al present was in IV-coordination), whereas $0.5Na_2O{\cdot}2K_2O{\cdot}1.7CaO[KAlO_2{\cdot}(SiO_2)_{2.9}]_7{\cdot}yH_2O$ was found at the quartz surface only ~15 μm away within the same sample. In any case, the molar Si/Al ratio of the interfacial layer was approximately 2.5–3 at all aluminosilicate mineral surfaces examined, irrespective of the parent siliceous rocks. The molar Si/Al ratio of the bulk gel binder was ~2 with an averaged composition of $2.1Na_2O{\cdot}0.24MgO{\cdot}3CaO{\cdot}[Na_{0.15}K_{0.85}AlO_2{\cdot}(SiO)_{1.8}]_{20}{\cdot}0.5Fe_2O_3{\cdot}zH_2O$. The reason for this increased interfacial Si/Al ratio is still unknown, but may be better understood by examining the chemical interactions between aluminosilicate minerals and alkaline solution, with and without soluble silicates.

3.2. Chemical interactions between aluminosilicates and activating solutions

Natural siliceous rocks are mixtures of various mineral phases with varying proportions. To study such mixtures chemically at the level of detail required here is an extremely difficult task. Therefore, the chemical interactions between alkaline (silicate) solutions and two simple crystalline aluminosilicate minerals, clay (kaolinite, HR1 grade) and Na-feldspar (albite), are firstly examined. The results obtained from the pulverised basalt, which are averages of all the chemical interactions between the various mineral phases of basalt, will then be compared to these ideal systems in order to identify the similarities and differences between the chemical reactions taking place at the aluminosilicate-activating solution interface, which may shed some light on how the interfacial layer is formed in the alkali activated cement concrete systems of primary interest here.

3.2.1. Kaolinite

When kaolinite was suspended in alkaline solutions without additional soluble silicates (systems *Kao 1*, *3* and *5*), it was found that the initial Si dissolution was very rapid (Fig. 7). It is also evident from Fig. 7 that no Al dissolution was observed in the first 8 h in the 0.6 M MOH solution (*Kao 1*). This delay in the initiation of Al dissolution was also observed in solutions of higher solution alkalinities ($[OH^-]$=5 and 10 M, *Kao 3* and *5*), where the concentration of Si in the solution was always higher than Al (whereas the Si/Al ratio of the unreacted kaolinite ($Al_2Si_2O_5(OH)_4$) is 1), although the time required to observe the dissolved Al became shorter with increasing solution alkalinity. The dissolving kaolinite surface at this initial non-stoichiometric stage will therefore be depleted in Si and enriched in Al, which is consistent with a surface reaction-controlled mechanism — initial aluminosilicate dissolution is controlled by the Si-activated complexes ≡Si–O^- with a higher detachment rate of Si than Al [15,16].

After around 8 h of leaching, steady-state kaolinite dissolution was observed in systems *Kao 1*, *3* and *5*. Both Si and Al dissolution are in fact linear with time as shown in the inset to Fig. 7, however a logarithmic time axis is necessary in this plot and other leaching plots to display the full reaction time period. As batch reactors are not designed to avoid concentration build-up of the constituent metals of the dissolving mineral, the steady-state dissolution observed in this work suggests that the kaolinite dissolution may be zero order with respect to Si and Al. This implies that in the conditions of systems *Kao 1*, *3* and *5*, at least within the duration of this work, the steady-state dissolution kinetics of the kaolinite were not chemical affinity-controlled. Consequently, the zero-order kaolinite steady-state dissolution rates were calculated by ignoring the results obtained in the first 8 h of leaching as summarised in Table 3, in agreement with results obtained previously [16–18]. The fact that the dissolution rates of Si and Al were similar to each other suggests that the kaolinite dissolution in alkaline solutions

Table 3
The maximum apparent dissolutions and the zero-order dissolution rates, with respect to Si and Al, of kaolinite and albite in the activating solutions at 25 °C

System	Log (rate) (mole m^{-2} s^{-1})		Maximum apparent dissolution, mM, at (time, h) [a]	
	Si	Al	Si	Al
Kao 1	−11.28 [b]	−11.75 [b]	6.7 (168)	1.8 (168)
Kao 2	– [c]	−12.97 [b]	3.6 (168)	0.4 (168)
Kao 3	−10.80 [b]	−10.67 [b]	22.2 (168)	15.3 (168)
Kao 4	– [c]	−10.75 [b]	14.2 (48)	17.0 (168)
Kao 5	−10.23 [b]	−10.18 [b]	67.3 (168)	58.2 (168)
Kao 6	– [c]	−10.23 [b]	92.6 (4)	58.9 (168)
Alb 1	– [d]	– [d]	18.7 (168)	4.5 (168)
Alb 2	– [c]	– [e]	10.7 (168)	2.7 (168)
Alb 3	– [d]	– [d]	27.8 (168)	8.0 (168)
Alb 4	– [c]	– [d]	39.5 (96)	9.3 (168)
Alb 5	– [d]	– [d]	28.9 (168)	9.8 (168)
Alb 6	– [c]	– [d]	32.0 (48)	11.2 (168)

[a] Unless otherwise indicated, only dissolution was observed.
[b] Rate constants obtained by fitting the linear part of the dissolution curve. All R^2 values exceed 0.92.
[c] Both apparent dissolution and precipitation were significant.
[d] The dissolution rate was linear against log(time).
[e] The dissolution rate was linear against log(time) and then levelled off.

without additional soluble silicates was approximately stoichiometric or quasi-stoichiometric at the steady-state stage. As the Al dissolution rate was slightly higher than that of Si in *Kao 3* and *5* (Table 3), detachment of Al from the ≡Al–O$^-$ activated complexes was the rate-limiting step at the steady-state dissolution, as was also proposed by others [15,16].

As discussed above, aluminosilicate dissolution in highly alkaline environments should be controlled by the Si-activated complexes during the initial non-stoichiometric stage. According to Iler [19], the resulting Al-enriched gibbsite-like reacting surface [16] should act as an adsorbent towards soluble silicate, as was observed by Siever and Woodford [20]. With the assumption that the nature of the 'initial' reacting surface in the alkaline silicate solutions (*Kao 2*, *4* and *6*) and in the soluble silicate-free alkaline solutions (*Kao 1*, *3* and *5*) should be the same, it is expected that surface adsorption of the 0.5 M added soluble silicates should be observed in *Kao 2*, *4* and *6*, especially during the initial non-stoichiometric dissolution stage.

The effects of soluble silicate addition on the dissolution/precipitation characteristics of kaolinite are presented in Fig. 8. It was found that, at a solution alkalinity ($[OH^-]_0$) of 0.6 M and a soluble silicate dosage ($[SiO_2]_0$) of 0.5 M, in system *Kao 2*, some of the added soluble silicates were adsorbed by the Al-enriched kaolinite surface within the first 4 h of leaching. This is consistent with the above hypothesis. As the true dissolution of kaolinite was inhibited because of the soluble silicate adsorption (the apparent Al dissolution of kaolinite and the XRD intensity reduction of the kaolinite were reduced in the presence of soluble silicates, see Table 3 and Fig. 9), it is likely that the subsequent dissolution-dominant stage observed in *Kao 2* between 4 and 96 h could be largely attributed to the desorption of the initially adsorbed soluble silicates.

At $[OH^-]_0$=5 M and $[SiO_2]_0$=0.5 M (*Kao 4*), Si precipitation on the kaolinite surface was also observed within the first 2–4 h (Fig. 8), corresponding to the initial non-stoichiometric dissolution of *Kao 3* that produced an Al-enriched surface for soluble silicate adsorption. This was followed in *Kao 4* by a Si dissolution-dominant stage until ~48 h, which might include both the desorption of the adsorbed

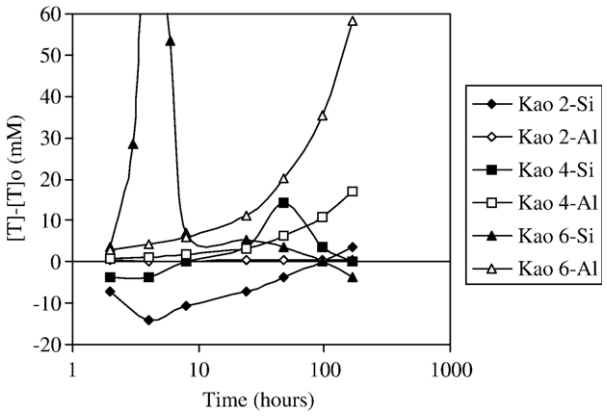

Fig. 8. Leaching behaviour of kaolinite in alkaline silicate solutions with $[SiO_2]$= 0.5 M and $[OH^-]$=0.6 M (*Kao 2*), 5 M (*Kao 4*) and 10 M (*Kao 6*). $[T]$= concentration of Si or Al in the solution, $[T]_0$= initial concentration of Si or Al in the leaching solution.

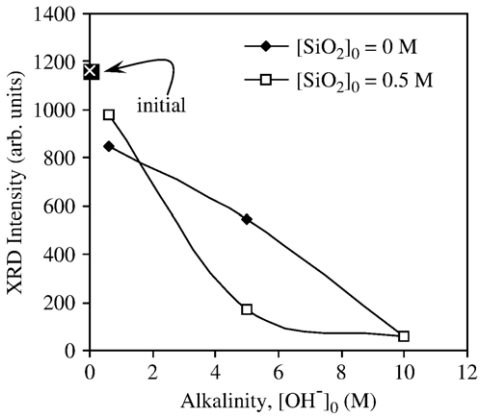

Fig. 9. XRD intensity of the kaolinite peak at *d*-spacing=7.183 Å after 168 h, as a function of the initial solution alkalinity in hydroxide and silicate solutions.

soluble silicates and the dissolution of the kaolinite. After ~48 h, the Si from the added soluble silicates and/or the dissolved kaolinite was then either adsorbed again by the kaolinite or reprecipitated as a new phase, as shown by the negative slope of the ($[Si]-[Si]_0$) versus time curve. This is possibly because the kaolinite reacting surface was once again saturated with Al-rich species. From the XRD analysis (Fig. 9), addition of 0.5 M soluble silicates was very effective in promoting structural change to the kaolinite crystalline structure at $[OH^-]_0$=5 M as the kaolinite peak at *d*-spacing=7.183 Å (and all other peaks due to the kaolinite structure) had almost completely disappeared in *Kao 4* at 168 h, whereas the intensity of the same peak was only reduced by about half in *Kao 3*. Kaolinite structural alteration in *Kao 4* started at least as early as 48 h (when the maximum apparent dissolution was observed, see Table 3), or earlier, according to the FTIR analysis in Fig. 10. The intensities of the kaolinite characteristic bands (see Table 4 for the detailed assignments [21–27]) were significantly reduced and broadened in *Kao 4* at 48 h, whereas the FTIR spectrum of *Kao 3* was almost the same as that of the unreacted kaolinite after 168 h. This is despite the fact that the maximum apparent dissolution of *Kao 4* observed at 48 h was only ~2% of the theoretical maximum value (excluding the dissolution of the silica impurity), showing that reprecipitation reactions must be playing a highly significant role in this system. The reacted solids were X-ray amorphous as no new crystalline peaks could be identified (not shown), and may be identified as resembling to a certain extent the aluminosilicate gel phase present in a geopolymeric gel system.

When the solution alkalinity was increased even higher to 10 M with 0.5 M soluble silicate (*Kao 6*), the initial precipitation-dominant stage of *Kao 2* and *Kao 4* was not observed. The chemical interactions between the kaolinite and the *Kao 6* activating solution were instead characterised by a dissolution-dominant stage from the start of the solution analysis (2 h) to ~4 h of leaching. Subsequently, the added and the dissolved Si were adsorbed by the reacted kaolinite and formed a secondary aluminosilicate phase, as shown by the negative slope of the leaching curve (Fig. 8). At this alkalinity, the effect of the soluble silicate addition on the kaolinite structural alteration

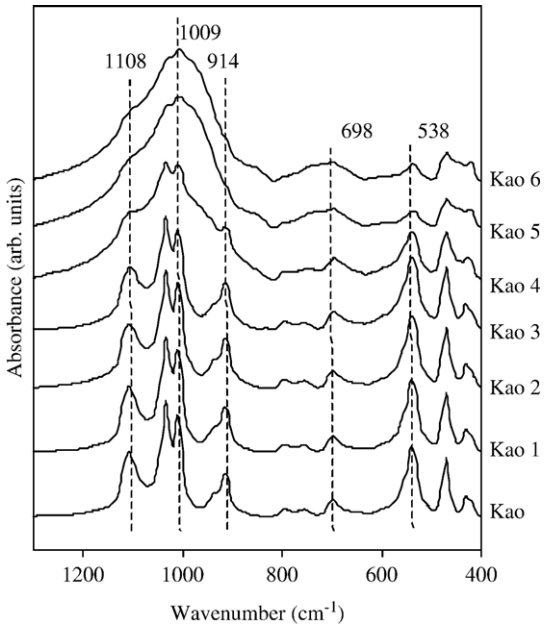

Fig. 10. Effect of leaching on the FTIR spectrum of kaolinite: unleached (*Kao*) and after exposure to different alkaline hydroxide (*Kao 1, 3, 5*) and silicate (*Kao 2, 4, 6*) solutions. All spectra were taken at the point of maximum dissolution (Table 3).

was not obvious from the XRD analysis. The kaolinite peak at *d*-spacing = 7.183 Å for both *Kao 5* and *6* was reduced to the same intensity level as the background intensity at 168 h. The FTIR analysis (Fig. 10), however, indicates that soluble silicates had accelerated the structural alteration process as the kaolinite characteristic bands at 1108, 1009, 914, 698, 538 and 435 cm^{-1} had completely disappeared and significantly broadened at the 4th hour of leaching in *Kao 6*, whereas 168 h were required for *Kao 5* to reach a similar extent of structural alteration.

3.2.2. Albite

The dissolution characteristics of albite in the various alkaline solutions (*Alb 1*, *3* and *5*) are summarised in Fig. 11. Throughout the present investigation, the albite dissolution was approximately linear against log (time) in the solutions of various alkalinities ($[OH^-]$ = 0.6, 5 and 10 M). According to Knauss and Wolery [28], it is necessary to react albite for ~14 days before steady-state dissolution similar to that of kaolinite (Fig. 7) can be reached, if a pH 10 solution at 25 °C is used. Hence, it is possible that the albite dissolution observed in this work could still be at the initial non-stoichiometric dissolution stage even until the end of the present experimental investigation (7 days).

From Fig. 11, it was also observed that the initial dissolution of Si was faster than that of Al in *Alb 1*, *3* and *5*, with consideration of the stoichiometric ratio of the unreacted ideal albite ($NaAlSi_3O_8$). The albite reacting surface should therefore be enriched with Al, as in the case of the kaolinite reacting surface. It therefore appears that when exposed to highly alkaline solutions ($[OH^-] \geq 0.6$ M or pH ≥ ~13.7), aluminosilicate mineral surfaces in general should be depleted in Si and enriched in Al by the end of the initial non-stoichiometric dissolution stage. Similar effects were also observed by Chou and Wollast [16] and Hamilton *et al*. [29], albeit at much lower solution alkalinities (pH = 9–11.24) than this work. The initial non-stoichiometric dissolution should therefore be controlled by the $\equiv Si{-}O^-$ complexes until steady-state dissolution is reached for all aluminosilicate minerals.

From Fig. 12, when albite was exposed to leaching solutions of 5 M or 10 M OH^- and 0.5 M (*Alb 4* and *Alb 6*), it was found that the effect of soluble silicate addition was dissimilar to that observed on the kaolinite using the same alkaline silicate solutions (*Kao 4* and *Kao 6*, see Figs. 7 and 8). For example, the initial precipitation of the added soluble silicates was not observed in *Alb 4*, which was otherwise the case in *Kao 4*. Nevertheless, the presence of soluble silicates still increased the maximum apparent Si dissolution of albite in both *Alb 4* and *Alb 6* within a shorter reaction time. See Table 3. After the maximum apparent Si dissolution was reached (at ~96 h for *Alb 4* and at ~48 h for *Alb 6*), a Si precipitation-dominant stage was then observed in *Alb 4* and *Alb 6* until the end of the present investigation.

From Fig. 12, it seems that the net amount of Si being adsorbed by the reacted albite, after the maximum apparent

Table 4
Characteristic IR vibrational bands of the solid raw materials

Wavenumber (cm^{-1})	Assignment	References
1108, 1033, 1009 (s)	Kaolinite Si–O in-plane vibration	[21]
1162, 1142, 1102, 1058, 1018, 997 (s)	Albite asymmetric stretching (Si–O–Si(Al))	[25,26]
980–960 (sh)	Si–O stretching ($Si–O^-M^+$)	[24]
1100–960 (sh)	Asymmetric stretching (Si–O–Al)	[25,26]
914 (s)	Kaolinite, OH bending (Al–OH)	[21]
781, 762, 744, 732 (m)	Albite, symmetric stretching (Si–O–Si(Al))	[25,26]
698 (m), 538 (sh)	Kaolinite, bending (Al–O–Si)	[21,24]
650, 611, 591 (s)	Albite, bending (O–Si(Al)–O)	[25,26]
550–400 (s)	Deformation (Si–O–Si and O–Si–O)	[21–27]

Abbreviations in parentheses: s = strong, w = weak, m = medium, and sh = shoulder.

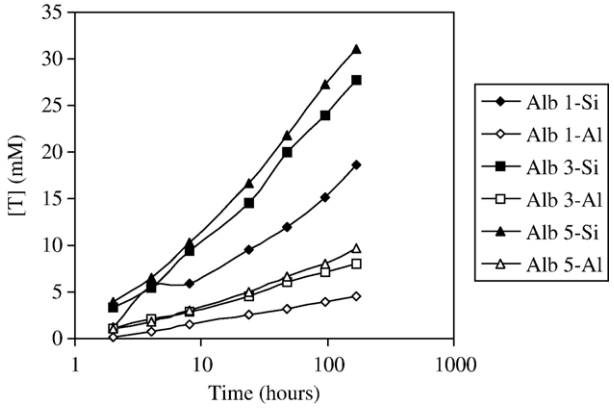

Fig. 11. Leaching behaviour of albite in alkaline hydroxide solutions with $[OH^-]$ = 0.6 M (*Alb 1*), 5 M (*Alb 3*) and 10 M (*Alb 5*). [*T*] = concentration of Si or Al in the solution.

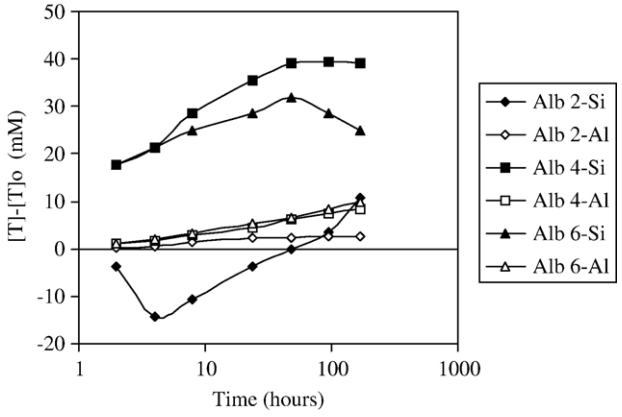

Fig. 12. Leaching behaviour of albite in alkaline silicate solutions with $[SiO_2]$= 0.5 M and $[OH^-]$=0.6 M (*Alb 2*), 5 M (*Alb 4*) and 10 M (*Alb 6*). [*T*]=concentration of Si or Al in the solution, $[T]_0$ =initial concentration of Si or Al in the leaching solution.

dissolution was observed, was greater in *Alb 6* than in *Alb 4*. This is confirmed by the FTIR and the SEM & EDS analyses as presented in Figs. 13 and 14 respectively. A new spectral band at 961 cm^{-1}, attributable to the stretching vibration of the Si–O bond from the $-SiO^-M^+$ (M=Na or K) group [24], or the asymmetric stretching vibration of the Si–O–Al bond within a highly Al-substituted aluminosilicate structure (consistent with the assumption that the Al-rich albite reacted surface should be an efficient adsorbent for soluble silicates) [25,26], was observed in the *Alb 6* leached albite but not in any other leached albite (Fig. 13). Furthermore, the spectral regions at around 760 cm^{-1} (attributable to symmetric stretching of Si–O–T, T=Si or Al [25,26]) and around 590 cm^{-1} (attributable to bending vibration of O–T–O [25,26]) had become broadened only in *Alb 6*, as if the albite had transformed from the crystalline state to a glassy state [22]. As the XRD analysis had failed to detect any structural change throughout any of the systems *Alb 1* to *6* (data not shown), it can be concluded that:

(1) the chemical interactions between albite and alkaline solutions only occurred at the albite surfaces, different from what was observed in the kaolinite systems;
(2) the spectral broadening at the 760 and 590 cm^{-1} regions in *Alb 6* was caused by the deposition of the dissolved and/or added soluble silicates onto the reacted albite surfaces; and
(3) the new 961 cm^{-1} band in the *Alb 6*-reacted albite should be assigned to the reacted albite surfaces having newly adsorbed silicate species from the surrounding solution, which according to the SEM-EDS analysis, should have an averaged chemical formula (from 5 separate analyses on 5 different locations) of approximately $0.19Na_2O \cdot 0.01K_2O \cdot [KAlO_2 \cdot (SiO_2)_3] \cdot mH_2O$.

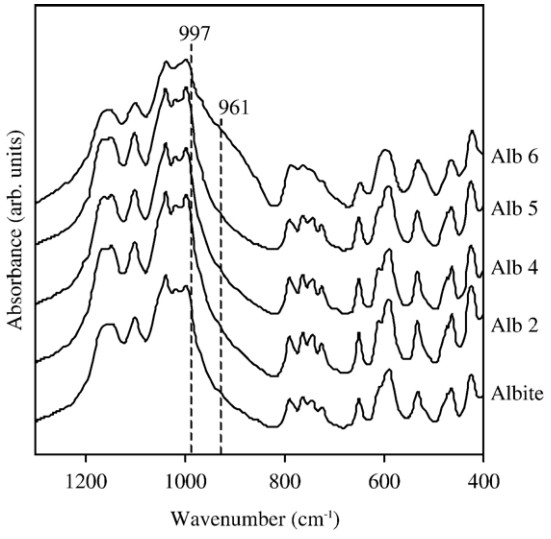

Fig. 13. Effect of leaching on the FTIR spectrum of albite: unleached and after exposure to different alkaline hydroxide (*Alb 5*) and silicate (*Alb 2, 4, 6*) solutions. All spectra were taken after 168 h.

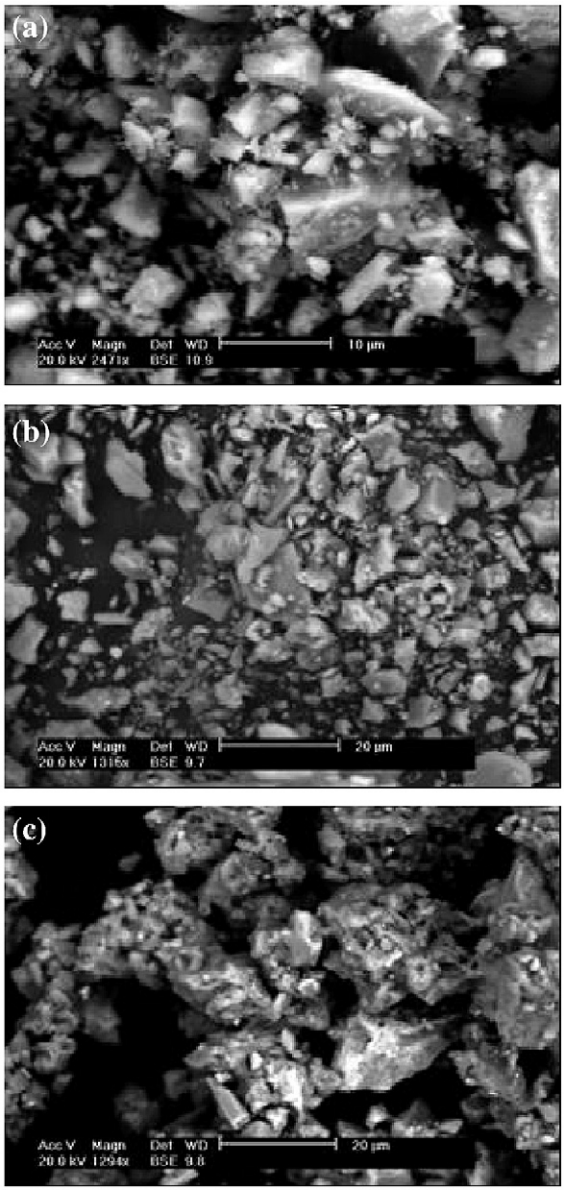

Fig. 14. BSE SEM images of (a) unreacted albite, (b) reacted albite from system *Alb 4* after 168 h, and (c) reacted albite from system *Alb 6* after 168 h.

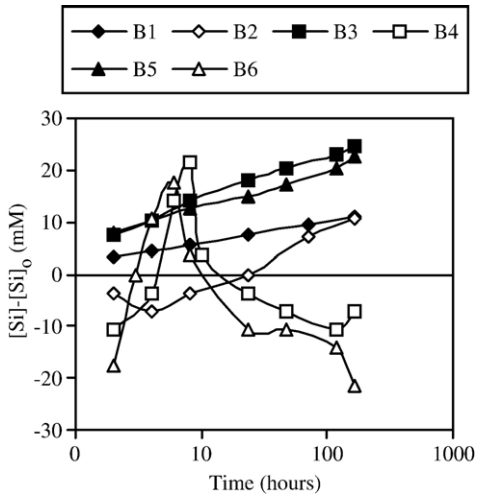

Fig. 15. The leaching curves of basalt in the various alkaline hydroxide (*B1, 3, 5*) and silicate (*B2, 4, 6*) solutions. [Si]=concentration of Si in the solution at time *t*. $[Si]_0$=initial concentration of Si in the leaching solution.

These newly formed aluminosilicates on the *Alb 6*-reacted albite surface, or the *Alb 6* interfacial layer, are likely to be responsible for holding the albite particles together to form conglomerates as shown in Fig. 14 (c), which were not observed in the unreacted albite (Fig. 14 (a)) or any other reacted albite (e.g. Fig. 14 (b)). This *Alb 6* interfacial layer could be similar in nature to the deposited aluminosilicate gel layer described by Phair *et al*. [30,31], where an aluminosilicate with a characteristic IR spectral band at 976 cm^{-1} (attributable to asymmetric stretching vibration of the Si–O–Al bond of an alkali-modified aluminosilicate with significant Al substitution [25,26,30]) was formed by suspending zirconia particles in sodium silicate and aluminate. According to Phair *et al*. [31], the formation of a deposited aluminosilicate layer on a relatively unreactive solid surface (zirconia) is more favourable at a higher solution alkalinity due to the greater concentrations of the hydrated cationic sites ($-ZrO^-M^+$) and/or monomeric soluble silicates being formed. The dissolution profiles of albite in *Alb 3* and *Alb 5* were similar (see Fig. 11 and Table 3) and the transition state theory (TST) [32] predicts that the rate of dissolution will be controlled by the formation of an activated complex. Therefore, the formation of the interfacial aluminosilicate layer in *Alb 6* should be attributed to the greater concentration of monomeric silicates present in *Alb 6*, and not to a greater extent of deprotonation of the surface silanol and/or aluminol groups in *Alb 6* than that of *Alb 4*.

Table 5
The maximum apparent dissolution extents of basalt in each activating solution at 25 °C

System	Maximum apparent dissolution, mM, at (time, h)				
	Si	Al	Ca	Mg	Fe
B 1	10.9 (168)	5.0 (168)	0.3 (168)	0.0	0.0
B 2	10.7 (168)	3.0 (24)	0.4 (168)	0.8 (168)	0.1 (168)
B 3	24.6 (168)	9.8 (168)	0.0	0.0	0.0
B 4	21.4 (8)	9.0 (168)	0.4 (24)	1.3 (168)	0.7 (168)
B 5	23.9 (168)	8.2 (168)	0.0	0.0	0.2 (168)
B 6	10.7 (4)	9.0 (168)	0.0	0.2 (4)	0.5 (168)

3.3. Chemical interactions between pulverised siliceous rocks and activating solution

From Fig. 15 and Table 5, it was found that the general leaching characteristics of the pulverised basalt in the various activating solutions were similar to what was observed in the systems containing kaolinite and albite (see Figs. 7, 8, 11 and 12 and Table 3). In alkaline solutions without soluble silicates (*B 1*, *3* and *5*), the dissolution of Si and Al from the basalt was continuous without apparent precipitation. On the other hand, when 0.5 M soluble silicates were added, the chemical interactions between the pulverised basalt and the alkaline silicate solutions (*B 2*, *4* and *6*) were characterised by an initial Si precipitation-dominant stage, where the added soluble silicates were adsorbed by the pulverised basalt. This was followed by a Si dissolution dominant stage, within which the adsorbed soluble silicates might be desorbed together with the dissolution of the basalt (similar to *Kao 2*, *4* and *6* and *Alb 2*, *4* and *6*). Note that at low solution alkalinity ($[OH^-]_0$=0.6 M, *B 2*), the second Si precipitation-dominant stage was not observed, as was the case also in *Kao 2* and *Alb 2*.

Similar to the formation of the *Alb 6* interfacial layer, the surface adsorption of the dissolved silicates onto the *B 4* and *B 6*-reacted basalt should be responsible for the formation of the interfacial layers that held the pulverised basalt particles together to form conglomerates as demonstrated in Fig. 16(b), which

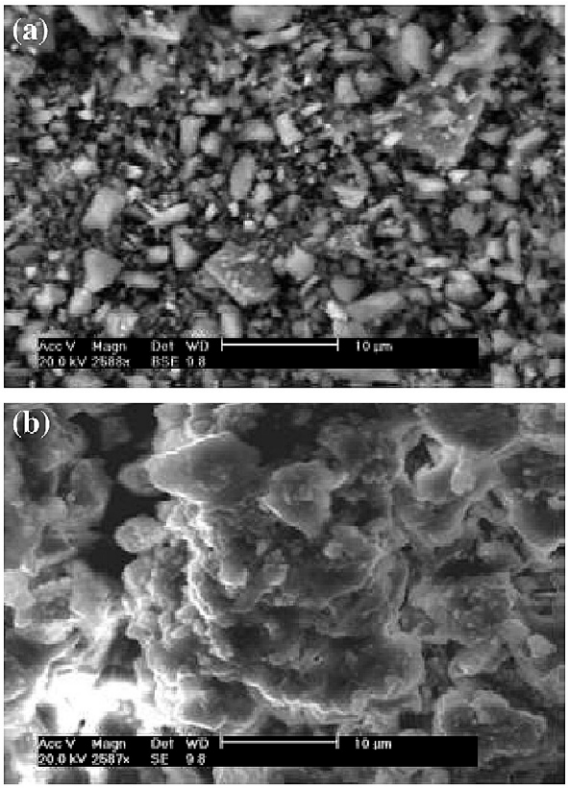

Fig. 16. SEM images of (a) unreacted pulverised basalt using BSE detection, and (b) reacted pulverised basalt from system *B6* after 168 h of reaction, using SE detection.

were absent in the unreacted pulverised basalt (Fig. 16(a)). The SEM-EDS analysis shows that the averaged chemical composition of the *B 4* interfacial layer was approximately $1.2Na_2O\cdot 0.8MgO\cdot[KAlO_2\cdot(SiO_2)_{2.9}]_6\cdot 1.7Fe_2O_3\cdot nH_2O$, whereas the *B 6* interfacial layer was lower in sodium, $0.6Na_2O\cdot MgO\cdot[KAlO_2\cdot(SiO_2)_{2.9}]_6\cdot 1.6Fe_2O_3\cdot pH_2O$. In comparison with the *Alb 6* interfacial layer, it seems that the interfacial layer formed by reacting the various aluminosilicates in the alkaline silicate solutions, in general, had a Si/Al ratio of ~3. This will obviously depend on the composition of the reactive phases in the fly ash used in alkali-activated cement synthesis, and so this will not be expected to be a universally applicable value. However, this value is similar to what was observed in the interfacial layer between the real siliceous rocks before pulverisation (basalt and siltstone) and the alkali-activated binder phase as presented previously. The interfacial layers of *Alb 6*, *B 4* and *B 6* are observed to be X-ray amorphous, as XRD diffractograms of all reacted solids resembled very closely those of the unreacted solids (data not shown).

The chemical interactions between albite or the real basaltic rock (either pulverised, which should show the averaged characteristics of all the mineral phases, or sliced to form sandwich specimens) and the various activating solutions or the alkali-activated binder, were found to share similar general characteristics (i.e. the leaching characteristics and the Si/Al ratios of the interfacial layers formed). It is therefore likely that the deposited aluminosilicate interfacial layer formation observed in the albite systems could be relevant to geopolymer gel binder adhesion to the real siliceous rocks, and therefore provides a useful model system whereby these interactions may be analysed. The deposited aluminosilicate interfacial layer formation is a result of soluble silicate-promoted heterogeneous reactions that consist of accelerated surface dissolution of Si and Al followed by Si precipitation processes (Figs. 11, 12 and 15). This implies that an activating solution consisting of high concentrations of alkali (MOH) and soluble silicates is an essential prerequisite for the formation of a strong interface between siliceous aggregates and an aluminosilicate geopolymeric gel binder, which is crucial to the overall macroscopic properties of low-Ca alkali-activated cement concretes. This hypothesis has been experimentally verified elsewhere [33]. It will be useful to test the above hypothesis on the interface formation mechanisms in alkali-activated cement concretes on the basis of more experimental data on other mineral phases using the experimental method presented in this paper.

4. Conclusion

Through a series of leaching experiments, it was found that addition of 0.5 M soluble silicates to an activating solution highly concentrated in alkalis ($[OH^-]_0$=5 to 10 M) facilitated the formation of an Al-enriched aluminosilicate surface through accelerated Si-preferential dissolution of the parent aluminosilicates. This Al-enriched solid surface was crucial for the subsequent deposition of the dissolved and/or the added soluble silicates from the activating solution, which then led to the formation of a deposited aluminosilicate interface with a Si/Al ratio of ~3, resembling the real interface between natural siliceous aggregates (basalt and siltstone) and a low-Ca alkali-activated cement, activated by a solution high in solution alkalinity ($[OH^-]_0$=10 M) and soluble silicates ($[SiO_2]_0$= 2.5 M). Without soluble silicates, no deposited aluminosilicate interface was observed either in the soluble silicate-free leaching or in the binder systems because the aluminosilicate surface was less Al-enriched and the dissolved Si concentration was too low to facilitate surface deposition. Furthermore, high solution alkalinity was found to promote deposited aluminosilicate interface formation because the activating solution was more concentrated in lower-order oligomeric soluble silicates, which was more preferable for heterogeneous soluble silicate deposition than a solution concentrated in larger silicate species. The results of this work suggest that both high concentrations of solution alkalinities and soluble silicates are essential for the formation of a strong interface between siliceous aggregates and low-Ca alkali-activated cements.

Acknowledgements

Financial support from the Australian Research Council (ARC) and the Particulate Fluids Processing Centre (PFPC), a Special Research Centre of the ARC, is gratefully appreciated.

References

[1] P. Duxson, A. Fernández-Jiménez, J.L. Provis, G.C. Lukey, A. Palomo, J.S.J. van Deventer, Geopolymer technology: The current state of the art, J. Mater. Sci., in press, doi:10.1007/s10853-10006-10637-z.
[2] J.G.S. van Jaarsveld, J.S.J. van Deventer, The potential use of geopolymeric materials to immobilize toxic metals. I. Theory and applications, Miner. Eng. 10 (1997) 659–669.
[3] J.L. Provis, G.C. Lukey, J.S.J. van Deventer, Do geopolymers actually contain nanocrystalline zeolites? — A reexamination of existing results, Chem. Mater. 17 (2005) 3075–3085.
[4] D.M. Roy, Alkali-activated cements: opportunities and challenges, Cem. Concr. Res. 29 (1999) 249–254.
[5] C.K. Yip, G.C. Lukey, J.S.J. van Deventer, Effect of blast furnace slag addition on microstructure and properties of metakaolinite geopolymeric materials, Ceram. Trans. 153 (2003) 187–209.
[6] K. Dombrowski, A. Buchwald, M. Weil, The influence of calcium content on the structure and thermal performance of fly ash based geopolymers, J. Mater. Sci., in press, doi:10.1007/s10853-006-0532-7.
[7] A. Palomo, A. Fernández-Jiménez, G.Y. Kovalchuk, L.M. Ordoñez, M.C. Naranjo, OPC-fly ash cementitious systems. Study of gel binders formed during alkaline hydration, J. Mater. Sci., in press, doi:10.1007/s10853-006-0585-7.
[8] M.R. de Rooij, Syneresis in Cement Paste Systems, PhD Thesis, Delft University Press, The Netherlands, 2000.
[9] L. Struble, J. Skalny, S. Mindess, A review of the cement-aggregate bond, Cem. Concr. Res. 10 (1980) 277–286.
[10] P.J.M. Monteiro, J.C. Maso, J.P. Ollivier, The aggregate-mortar interface, Cem. Concr. Res. 15 (1985) 953–958.
[11] B.D. Barnes, S. Diamond, W.L. Dolch, Hollow shell hydration of cement particles in bulk cement paste, Cem. Concr. Res. 8 (1978) 263–271.
[12] W.A. Tasong, J.C. Cripps, C.J. Lynsdale, Aggregate-cement chemical interactions, Cem. Concr. Res. 28 (1998) 1037–1048.
[13] R. Zimbelmann, A contribution to the problem of cement-aggregate bond, Cem. Concr. Res. 15 (1985) 801–808.
[14] W.K.W. Lee, J.S.J. van Deventer, Structural reorganisation of class F fly ash in alkaline silicate solutions, Colloids Surf., A Physicochem. Eng. Asp. 211 (2002) 49–66.

[15] P.V. Brady, J.V. Walther, Controls on silicate dissolution rates in neutral and basic pH solutions at 25 °C, Geochim. Cosmochim. Acta 53 (1989) 2823–2830.
[16] L. Chou, R. Wollast, Study of the weathering of albite at room temperature and pressure with a fluidized bed reactor, Geochim. Cosmochim. Acta 48 (1984) 2205–2217.
[17] F.J. Huertas, L. Chou, R. Wollast, Mechanism of kaolinite dissolution at room temperature and pressure Part II: Kinetic study, Geochim. Cosmochim. Acta 63 (1999) 3261–3275.
[18] J. Ganor, J.L. Mogollón, A.C. Lasaga, The effect of pH on kaolinite dissolution rates and on activating energy, Geochim. Cosmochim. Acta 59 (1995) 1037–1052.
[19] R.K. Iler, The Chemistry of Silica, John Wiley & Sons Publishers, New York, 1979.
[20] R. Siever, N. Woodford, Sorption of silica by clay minerals, Geochim. Cosmochim. Acta 37 (1973) 1851–1880.
[21] S. Olejnik, L.A.G. Aylmore, A.M. Posner, J.P. Quirk, Infrared spectra of kaolin mineral — dimethyl sulfoxide complexes, J. Phys. Chem. 71 (1968) 241–249.
[22] B. Velde, R. Couty, High-pressure infrared spectra of some silicate glasses, Chem. Geol. 62 (1987) 35–41.
[23] M. Zhang, B. Wruck, A.G. Barber, E.K.H. Salje, M.A. Carpenter, Phonon spectra of alkali feldspars: phase transitions and solid solutions, Am. Mineral. 81 (1996) 92–104.
[24] T. Uchino, T. Sakka, M. Iwasaki, Interpretation of hydrated states of sodium silicate glasses by infrared and Raman analysis, J. Am. Ceram. Soc. 74 (1991) 306–313.
[25] B.N. Roy, Spectroscopic analysis of the structure of silicate glasses along the joint of $xMAlO_2-(1-x)SiO_2$ (M=Li, Na, K, Rb, Cs), J. Am. Ceram. Soc. 70 (1987) 183–192.
[26] K. Sinko, R. Mezei, J. Rohonezy, P. Fratzl, Gel structures containing Al(III), Langmuir 15 (1999) 6631–6636.
[27] M. Handke, W. Mozgawa, M. Nocuń, Specific features of the IR spectra of silicate glasses, J. Mol. Struct. 325 (1994) 129–136.
[28] K.G. Knauss, T.J. Wolery, Dependence of albite dissolution kinetics on pH and time at 25 °C and 70 °C, Geochim. Cosmochim. Acta 50 (1986) 2481–2597.
[29] J.P. Hamilton, C.G. Pantano, S.L. Brantley, Dissolution of albite glass and crystal, Geochim. Cosmochim. Acta 64 (2000) 2603–2615.
[30] J.W. Phair, J.S.J. van Deventer, J.D. Smith, Interaction of sodium silicate with zirconia and its consequences for polysialation, Colloids Surf., A Physicochem. Eng. Asp. 182 (2001) 143–159.
[31] J.W. Phair, J.S.J. van Deventer, J.D. Smith, Mechanism of polysialation in the incorporation of zirconia into fly ash-based geopolymers, Ind. Eng. Chem. Res. 39 (2000) 2925–2934.
[32] H. Eyring, The activated complexes in chemical reactions, J. Chem. Phys. 3 (1935) 107–120.
[33] W.K.W. Lee, J.S.J. van Deventer, The interface between natural siliceous aggregates and geopolymers, Cem. Concr. Res. 34 (2004) 195–206.